

Article

Numerical Study of a Reconfigurable Multiband Microwave Photonic Filter Using a Tunable Fabry-Perot Filter

Blaise Tshibangu-Mbuebue ¹, Roberto Rojas Laguna ², Min Won Lee ³, Jorge Rodríguez-Asomoza ⁴ and Ignacio Enrique Zaldívar-Huerta ^{1,*} 

¹ Departamento de Electrónica, Instituto Nacional de Astrofísica, Óptica y Electrónica, Calle Luis Enrique Erro No. 1, Tonantzintla, Puebla 72840, Mexico; bmbuebue@inaoep.mx

² Departamento de Electrónica, División de Ingenierías Campus Irapuato-Salamanca, Universidad de Guanajuato, Carretera Salamanca-Valle de Santiago km 3.5 + 1.8, Salamanca 36885, Mexico; rlaguna@ugto.mx

³ Laboratoire de Physique des Lasers (UMR CNRS 7538), Université Sorbonne Paris Nord, 93430 Villetaneuse, France; min.lee@univ-paris13.fr

⁴ Departamento de Ingeniería en Computación, Electrónica y Mecatrónica, Universidad de las Américas-Puebla, Ex-Hacienda Santa Catarina Mártir, Cholula, Puebla 72820, Mexico; jorge.rodriguez@udlap.mx

* Correspondence: zaldivar@inaoep.mx

Abstract: Microwave photonic filters (MPFs) with the capabilities of bandwidth reconfigurability and frequency tunability in the GHz range are of great interest in high-speed communications systems. In this paper, we propose a new reconfigurable multiband microwave photonic filter (MPF) using a tunable Fabry–Perot Filter (FPF). It is demonstrated by numerical simulations that the modification of the intermodal separation ($\delta\lambda$) of a multimode laser diode (MLD) by tunable FPF allows for the reconfigurable multi-passband of the MPF. Our simulation results show that our new filter system is promising to communications systems.

Keywords: microwave photonic filter; microwave signals; Fabry-Perot filter; VPIphotonics software



Citation: Tshibangu-Mbuebue, B.; Rojas Laguna, R.; Lee, M.W.; Rodríguez-Asomoza, J.; Zaldívar-Huerta, I.E. Numerical Study of a Reconfigurable Multiband Microwave Photonic Filter Using a Tunable Fabry-Perot Filter. *Electronics* **2021**, *10*, 1473. <https://doi.org/10.3390/electronics10121473>

Academic Editor: Deep Jariwala

Received: 20 May 2021

Accepted: 3 June 2021

Published: 19 June 2021

Publisher's Note: MDPI stays neutral with regard to jurisdictional claims in published maps and institutional affiliations.



Copyright: © 2021 by the authors. Licensee MDPI, Basel, Switzerland. This article is an open access article distributed under the terms and conditions of the Creative Commons Attribution (CC BY) license (<https://creativecommons.org/licenses/by/4.0/>).

1. Introduction

At the present time, the delivery of services, such as the Internet, High-Definition Television (HDTV), data, etc., to the final user has begun to migrate to systems based on the use of optical fibers. In this technology, electrical signals are transmitted using photonic devices and optical fiber. This multidisciplinary field is possible thanks to high-speed photonic devices operating at microwave or millimeter-wave frequencies in microwave photonic systems [1]. In this regard, the MPFs are to be applied within microwave photonic technology. Potential applications of an MPF include the distribution and transmission of microwave signals via broadband optical links. Multiband MPFs have become excellent candidates with their inherent advantages from photonic technologies, such as their low loss, high bandwidth, high tunability, and high reconfigurability [2,3]. They are also attractive in optical communication systems because they can be used as electrical carriers to transmit information [4]. Currently, the tunability and reconfigurability of the frequency response of an MPF is a great topic of interest for researchers. For instance, a novel MPF was proposed based on a tunable ultra-sharp roll-off optical filter to demonstrate a flexible MPF with a large reconfigurable bandwidth and a wide frequency tuning range [5]. In [6], a reconfigurable and tunable multiband MPF was also developed, and flexible amplitudes and phase controls of the filter were achieved via optical spectral slicing by means of a programmable sampling function. A reconfigurable and application-specific tunable MPF with finite impulse response was also reported [7]. This filter exploits the differential mode group delays of linearly polarized modes in a multi-mode fiber to achieve single and multiple high-frequency passband responses. In our previous report, we proposed a tunable filter with a section of birefringent optical fiber placed between two crossed

polarizers in order to modify the optical spectrum of an MLD. Thanks to the fiber, the intermodal separation ($\delta\lambda$) is varied. Therefore, it allows for reconfigurability in the frequency of an MPF. However, the drawback of this filter is the birefringent fiber itself. When a particular passband is needed, it is necessary to use a particular length of fiber. In this new work, we propose a reconfigurable MPF using a tunable FPF in a dynamic way. The free spectral range (FSR) of the FPF is modified by an applied voltage, thus adjusting the intermodal separation $\delta\lambda$ of the MLD. In this way, reconfigurability in the frequency of the MPF is achieved. In this work, we study the feasibility of the reconfigurable MPF in the frequency range of 0–12 GHz. Due to the COVID-19 pandemic, we study this only by means of simulation using VPIphotonics software (Version 11.1, VPIphotonics GmbH, Berlin, Germany) [8]. The rest of this paper is organized as follows. The operation principles of an FPF and the MPF used in this work are described in Section 2. The simulation results of reconfigurability of the passbands by using a tunable FPF are shown in Section 3. Finally, conclusions are given in Section 4.

2. Brief Principle of Operation of an FPF and the MPF

In order to familiarize the reader with the basic operation of an FPF and an MPF, this section is devoted to explaining the basic principle of an FPF first, followed by that of the MPF.

2.1. Principle of Operation of an FPF

An FPF consists of a cavity formed by an index material refraction n embedded between two parallel flat and highly reflective mirrors, separated by a distance d . This filter possesses one input and one output port, the mirrors of which constitute the resonating cavity creating the multiple-beam interference process. Modification of the spacing between the mirrors can be done manually and/or electro-mechanically. The fastest tuning is achieved by means of a piezo actuator. The modification of spacing generates a tunable filter. The function transfer of the FPF in terms of optical power is given as [9].

$$T(f) = \frac{(1 - A - R)^2}{(1 - R)^2 + 4R_s \sin^2\left(\frac{\pi f}{FSR}\right)} \quad (1)$$

where A represents the signal losses within each mirror, R is the optical power reflectivity, $FSR = 1/2\tau$, with $\tau = nd/c$, which is the time it takes for the signal to propagate from one cavity mirror to the other, and c is the speed of light in a vacuum. Figure 1 shows the transfer function of the FPF that is composed of a sequence of maximum resonances that satisfy the transmission condition [10].

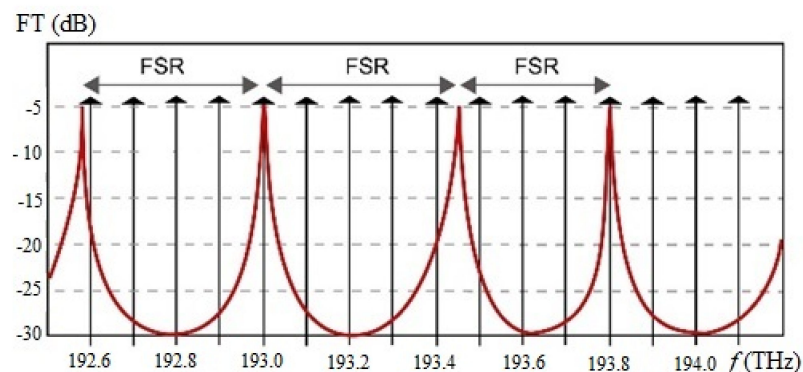


Figure 1. Periodic transmittance of an FPF.

The distance between two successive peaks is known as the free spectral range (FSR), also called axial mode spacing. In this work, varying the FSR of the simulated FPF allows

for the selection of specific optical modes from the multi-modes optical source. As a consequence, the adjustment of $\delta\lambda$ parameter in a dynamic way is achieved.

2.2. Principle of Operation of the MPF

Figure 2 shows the basic scheme of the passband MPF used in this work. Essentially, it is formed by a multimode laser diode (MLD), an electro-optic Mach–Zehnder intensity modulator (MZ-IM), an optical link of single-mode standard fiber (SM-SF), and a fast photodetector (PD).

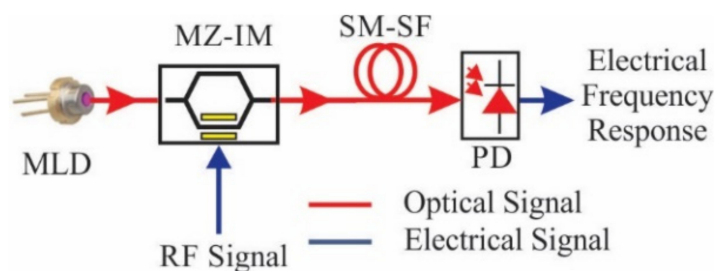


Figure 2. Basic scheme of the passband MPF used in this work.

When the SM-SF is dispersive to the wavelength used, the frequency response of the system is composed of a series of filtered signals or microwave passbands windows [11]. These passband windows are generated by considering the $\delta\lambda$ parameter of the MLD, the length (L) of the optical fiber, and its associated chromatic dispersion parameter (D). The corresponding value to the central frequency of the n th filtered microwave band-pass windows can be determined by the equation [11].

$$f_n = \frac{n}{DL\delta\lambda} \quad (2)$$

where $n = 1, 2, 3 \dots$

From Equation (2), it is evident that modifying the $\delta\lambda$ parameter allows for reconfigurability in the frequency of the filtered microwave band-pass windows. To illustrate this parameter, Figure 3 shows a typical optical spectrum of a commercial MLD (NX7538BF-AA, Renesas Electronics, Santa Clara, CA, USA) characterized by $\delta\lambda = 0.40$ nm. The inset depicts a magnified central zone showing the $\delta\lambda$ parameter in detail.

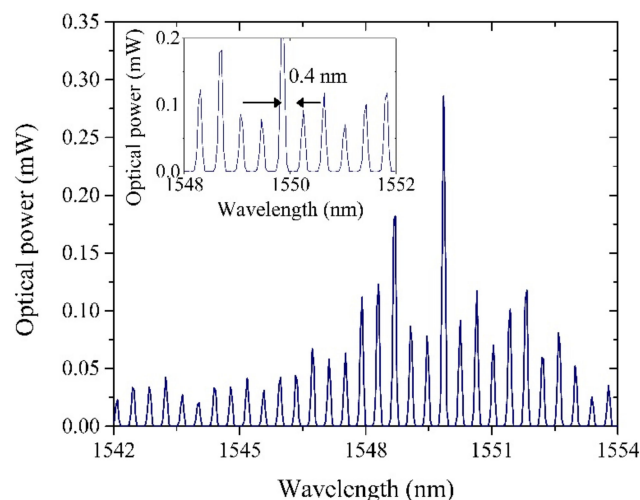


Figure 3. Optical spectrum corresponding to the MLD NX7538BF-AA.

3. Simulation and Results

VPIphotonics software is a simulation package that possesses a powerful simulation environment for the design, testing, and optimization of virtually any type of optical link. Its library is composed of active and passive integrated photonics devices, different types of optical sources and fibers, microwave electrical devices, optical and virtual electrical analyzers, among other things. It is very important to indicate that the parameters used in these simulations are adjusted to the optical characteristics of the devices available at our laboratory, considering that in the future it will be possible to carry out the experiments in the future. Unless otherwise indicated, the parameters $L = 13$ km and $D = 16.75$ ps/nm·km are maintained in the following. Figure 4 illustrates the layout implemented in VPIphotonics that corresponds to the scheme of Figure 2.

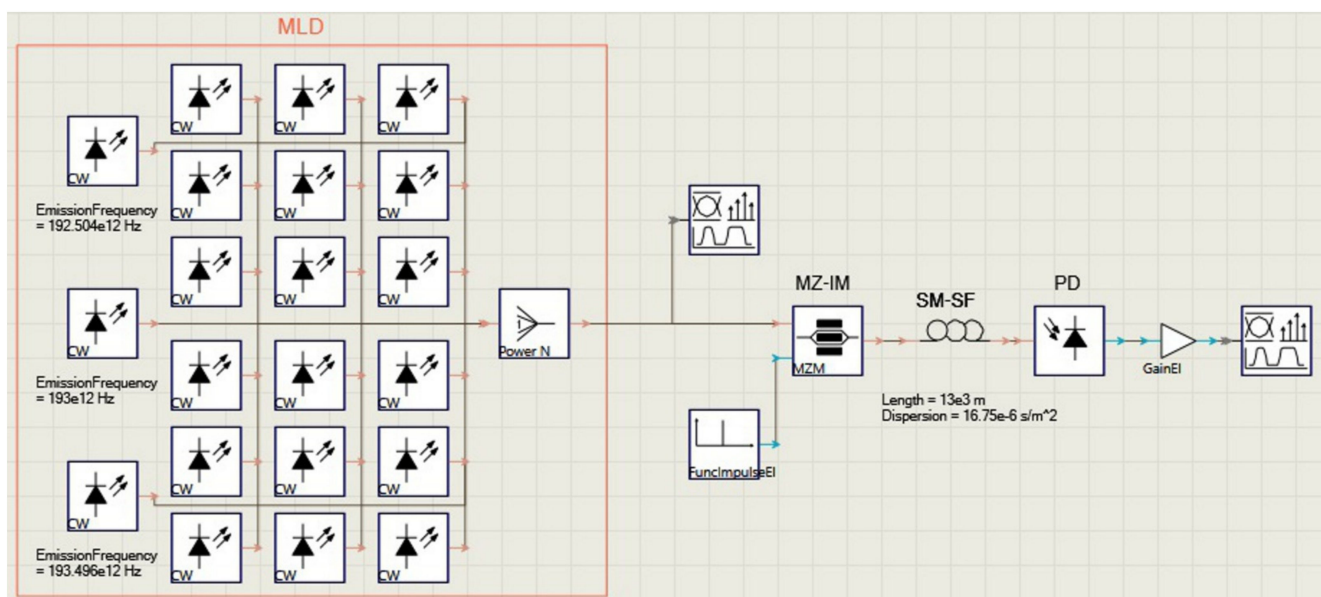


Figure 4. Layout of the simulated MPF in VPIphotonics software to obtain the filtering of microwave signals.

Figure 5 shows the result of simulation, considering $\delta\lambda = 0.40$ nm. Note the presence of a well-formed passband centered at $f = 11.26$ GHz exhibiting a bandwidth at -3 dB of $\Delta f_{bp} = 488.28$ MHz.

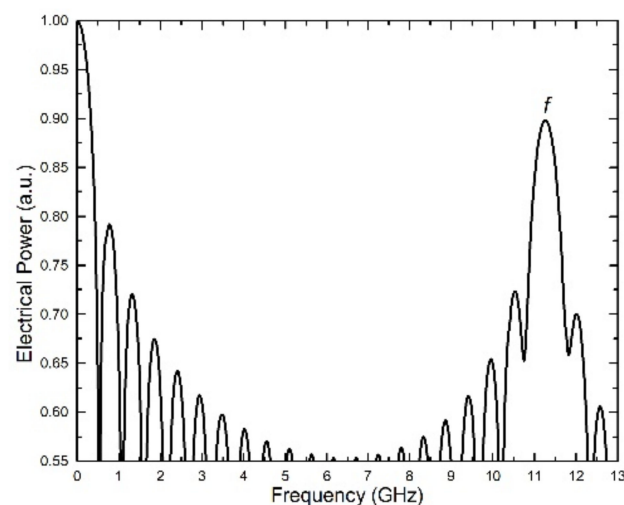


Figure 5. Simulated frequency response of the MPF corresponding to $\delta\lambda = 0.40$ nm value.

The next step is to generate the filtering of microwave signals below 11.26 GHz. For this purpose, the layout shown in Figure 6 is implemented. Here, a tunable FPF is inserted between the MLD and the MZ-IM. In this work, two values of FSR are used: $FSR = 100$ GHz for $\delta\lambda = 0.82$ nm, and $FSR = 200$ GHz for $\delta\lambda = 1.61$ nm.

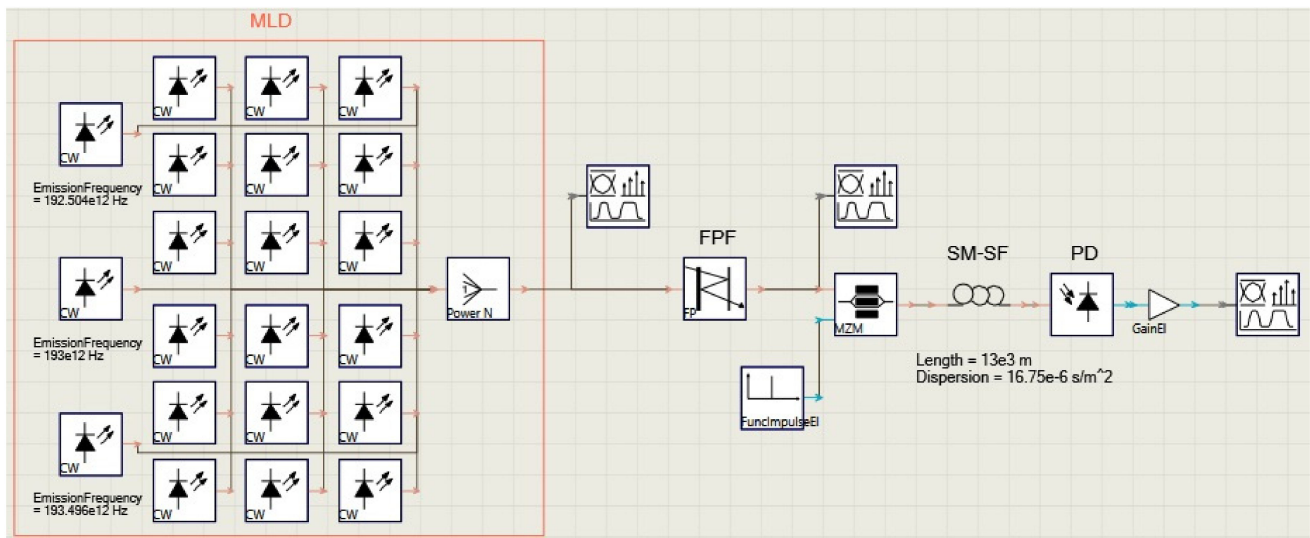


Figure 6. Layout of the simulated MPF in VPIphotonics software where a tunable FPF has been placed to modify the $\delta\lambda$ parameter.

Figure 7 shows the frequency response of the MPF with $FSR = 100$ GHz ($\delta\lambda = 0.82$ nm) in the blue curve and $FSR = 200$ GHz ($\delta\lambda = 1.61$ nm) in the red curve. In the case of $\delta\lambda = 0.82$ nm, a new passband $f_1 = 5.64$ GHz is observed; its value corresponds to a sub-multiple of the initial frequency of 11.26 GHz. Thus, two passbands at $f_1 = 5.64$ GHz and $f_2 = 11.26$ GHz are generated and their bandwidths at -3 dB are measured as $\Delta f_{bp1} = \Delta f_{bp2} = 488.28$ MHz.

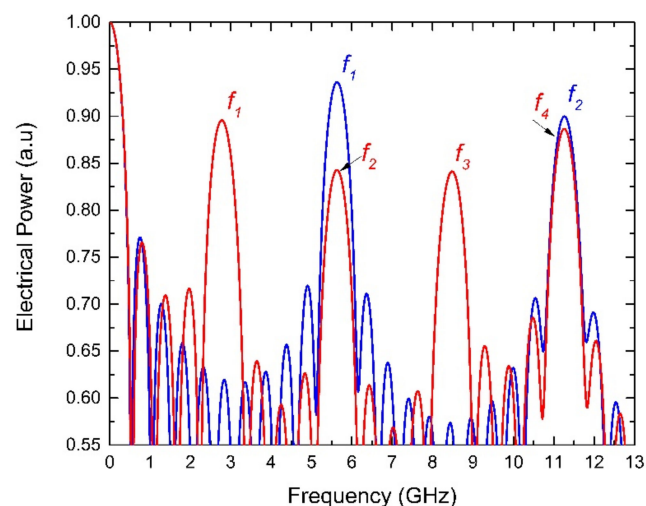


Figure 7. Simulated frequency response of the MPF corresponding to $\delta\lambda = 0.82$ nm (blue curve), and $\delta\lambda = 1.61$ nm (red curve).

For $\delta\lambda = 1.61$ nm, four passbands are observed at $f_1 = 2.77$ GHz, $f_2 = 5.64$ GHz, $f_3 = 8.47$ GHz, and $f_4 = 11.26$ GHz, as seen on the red curve in Figure 7. Its bandwidths at -3 dB are $\Delta f_{bp1} = \Delta f_{bp2} = \Delta f_{bp3} = \Delta f_{bp4} = 488.28$ MHz.

Now, the length of the optical fiber is set to $L = 25$ km and a set of simulations are conducted again with the same parameters. Figure 8 shows the results for these cases. In

the case of $\delta\lambda = 0.82$ nm ($FSR = 100$ GHz), three passbands are observed at $f_1 = 2.92$ GHz, $f_2 = 5.87$ GHz, and $f_3 = 8.78$ GHz (blue curve). For $\delta\lambda = 1.61$ nm ($FSR = 200$ GHz), seven passbands are observed at $f_1 = 1.44$ GHz, $f_2 = 2.92$ GHz, $f_3 = 4.41$ GHz, $f_4 = 5.87$ GHz, $f_5 = 7.30$ GHz, $f_6 = 8.78$ GHz, and an incipient $f_7 = 10.25$ GHz (red curve). In all of the cases, their measured bandwidths at -3 dB are $\Delta f_{bp} = 253.9$ MHz.

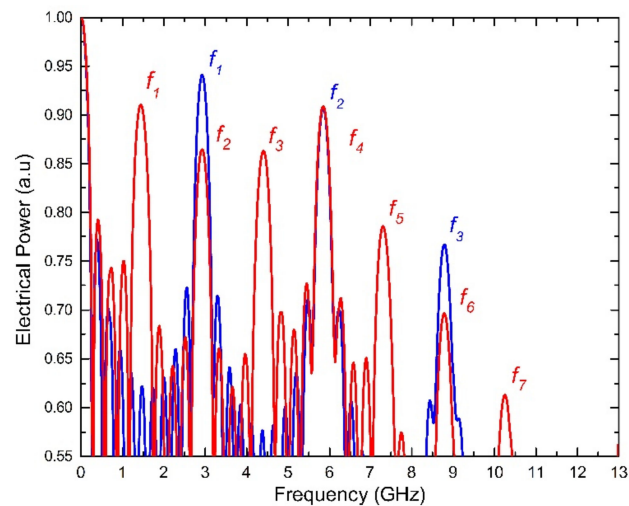


Figure 8. Simulated frequency response of the MPF corresponding to the use of $\delta\lambda = 0.82$ nm (blue curve), and $\delta\lambda = 1.61$ nm (red curve).

The passband frequencies are listed together with those calculated by Equation (2) in Table 1. For the sake of comparison, the previous results are also listed. It is clearly shown in the table that the numerical and theoretical values are in a good agreement.

Table 1. Summary of results.

| $L = 13$ km, $D = 16.75$ ps/nm·km | | | | | | | |
|-----------------------------------|----------------|----------------|----------------|----------------|----------------|----------------|----------------|
| - | f_1 (GHz) | f_2 (GHz) | f_3 (GHz) | f_4 (GHz) | - | - | - |
| $\delta\lambda = 0.40$ nm | 11.26 | - | - | - | - | - | - |
| Computed by Equation (2) | 11.48 | - | - | - | - | - | - |
| $\delta\lambda = 0.82$ nm | 5.64 | 11.26 | - | - | - | - | - |
| Computed by Equation (2) | 5.60 | 11.20 | - | - | - | - | - |
| $\delta\lambda = 1.61$ nm | 2.77 | 5.64 | 8.47 | 11.26 | - | - | - |
| Computed by Equation (2) | 2.85 | 5.70 | 8.55 | 11.40 | - | - | - |
| $L = 25$ km, $D = 16.75$ ps/nm·km | | | | | | | |
| - | f_1 (GHz) | f_2 (GHz) | f_3 (GHz) | f_4 (GHz) | f_5 (GHz) | f_6 (GHz) | f_7 (GHz) |
| $\delta\lambda = 0.40$ nm | 5.95 | - | - | - | - | - | - |
| Computed by Equation (2) | 5.97 | 11.94 | - | - | - | - | - |
| $\delta\lambda = 0.82$ nm | 2.92 | 5.87 | 8.78 | - | - | - | - |
| Computed by Equation (2) | 2.91 | 5.82 | 8.73 | 11.64 | - | - | - |
| $\delta\lambda = 1.61$ nm | 1.44 | 2.92 | 4.41 | 5.87 | 7.30 | 8.78 | 10.25 |
| Computed by Equation (2) | 1.48 | 2.96 | 4.44 | 5.93 | 7.41 | 8.89 | 10.38 |

4. Conclusions

In this paper, we have successfully demonstrated, at the simulation level, a proposal of reconfigurability in the frequency of a passband MPF. This reconfigurability was based on the use of a tunable FPF. It was demonstrated that the modification of the FSR parameter of the FPF allows for changes to the intermodal separation ($\delta\lambda$) of the MLD used as an optical source. This proposal was supported by a series of simulations by means of the VPIphotonics software. Reconfigurability of the passband was validated in the frequency range of 0–12 GHz. Simulation results are in good agreement with the theoretical values

computed by the use of Equation (2). Furthermore, it was demonstrated that this proposal of reconfigurability can be easily adapted to other values of L and $\delta\lambda$ parameters. It is remarkable that, as the length of the optical link was increased, the number of passbands was increased too. However, its electrical bandwidth was reduced. Nevertheless, this reduction is not critical because it is enough to code, for example, an analog signal in these passband windows for its transmission. As was established at the beginning of this paper, the filtering of passband windows is attractive in optical communication systems because they can be used as electrical carriers to transmit information coded on them. Now, with the obtained results, the versatility of the MPF analyzed in this work has been improved by selecting a particular passband window by appropriate manipulation of the FPF. As future work, once our laboratories open, we could corroborate our proposal with experimental results. For future experimental demonstration, we are going to use a tunable Fabry–Perot filter, which is thermally stable. In order to improve the frequency stability, it will be placed in a thermally insulated box. We will also study the frequency stability of our tunable MPF over time. In practice, the FSR will be controlled by the voltage applied to the piezoelectric electrode of the FPF. In summary, the main advantage of this proposal resides in the fact that the intermodal separation can readily be adjusted in a dynamical way by using a tunable FPF and, as a consequence, the reconfigurability in the frequency of a passband MPF. Furthermore, if the optical signal delivered by the photodetector is fed back by means of electrical components (passband filter and amplifier) to the electro-optic modulator, an optoelectronic oscillator configuration can be generated, and its tunability can also be achieved by means of the use of the Fabry–Perot filter.

Author Contributions: Conceptualization and methodology, R.R.L., J.R.-A., M.W.L. and I.E.Z.-H.; software, B.T.-M.; validation, R.R.L., I.E.Z.-H. and M.W.L.; formal analysis, I.E.Z.-H. and M.W.L.; investigation, B.T.-M.; resources, M.W.L. and I.E.Z.-H.; data curation, B.T.-M.; writing—original draft preparation, B.T.-M.; writing—review and editing, M.W.L. and I.E.Z.-H.; visualization, B.T.-M.; supervision, M.W.L. and I.E.Z.-H.; project administration, M.W.L. and I.E.Z.-H.; funding acquisition, M.W.L. and I.E.Z.-H. All authors have read and agreed to the published version of the manuscript.

Funding: This research received no external funding.

Acknowledgments: B.T.-M. wishes to thank to the Mexican Consejo Nacional de Ciencia y Tecnología (CONACyT) for the student scholarship number 846218. M.W.L. and I.E.Z.-H. thank the ECOS-Nord project (No. 299017).

Conflicts of Interest: The authors declare no conflict of interest.

References

1. Yao, J. Microwave Photonics. *J. Light. Technol.* **2009**, *27*, 314–335. [[CrossRef](#)]
2. Capmany, J.; Ortega, B.; Pastor, D. A tutorial on microwave photonic filters. *J. Light. Technol.* **2006**, *24*, 201–229. [[CrossRef](#)]
3. Yao, J. Photonics to the Rescue: A Fresh Look at Microwave Photonic Filters. *IEEE Microw. Mag.* **2015**, *16*, 46–60. [[CrossRef](#)]
4. Correa-Mena, A.G.; Vera-Marquina, A.; García-Juárez, A.; Rodríguez-Asomoza, J.; Zaldívar-Huerta, I.E. Experimental Transmission of Digital Data Coded on Electrical Carriers at 2.1 GHz and 4.2 GHz by Using a Microwave Photonic Filter. *Electronics* **2020**, *9*, 833. [[CrossRef](#)]
5. Ding, Z.; Zhao, J.; Yang, F.; Feng, Z.; Lu, B.; Cai, H. Wide Bandwidth Reconfigurable and Frequency Tunable Microwave Photonic Filter Based on Tunable Ultra-sharp Roll-off Optical Filter. In Proceedings of the 2018 Asia Communications and Photonics Conference (ACP), Hangzhou, China, 26–29 October 2018; pp. 1–3.
6. Liu, L.; Jin, X.; Ning, T.; Chen, L.R.; Capmany, J. Optical Spectral Slicing Based Reconfigurable and Tunable Microwave Photonic Filter. *J. Light. Technol.* **2020**, *38*, 5492–5499. [[CrossRef](#)]
7. Mirza, J.; Atieh, A.; Aljohani, A.J.; Ghafoor, S. Design and optimization of a microwave photonic filter exploiting differential mode group delay of a multi-mode fiber. *Opt. Rev.* **2021**, *28*, 199–206. [[CrossRef](#)]
8. Available online: <https://www.vpiphotonics.com/index.php> (accessed on 13 May 2021).
9. Kasap, S.O. *Optoelectronics and Photonics: Principles and Practices*; Prentice Hall: Hoboken, NJ, USA, 2001.
10. Venghaus, H. *Wavelength Filters in Fibre Optics*; Springer Nature: Cham, Switzerland, 2006.
11. González-Mondragón, L.; Quintero-Rodríguez, L.; García-Juárez, A.; Vera-Marquina, A.; Zaldívar-Huerta, I. Multiple passband microwave photonic filter with adjustable bandwidth. *Opt. Laser Technol.* **2020**, *126*, 106133. [[CrossRef](#)]